Proceedings of the International School and Conference on Photonics, PHOTONICA09

Hydrothermal Synthesis of CeO_2 and $Ce_{0.9}Fe_{0.1}O_2$ Nanocrystals

M. Radović[a,*], Z.D. Dohčević-Mitrović[a], A. Golubović[a], B. Matović[b], M. Šćepanović[a] and Z.V. Popović[a]

[a]Institute of Physics, Center for Solid State Physics and New Materials, Belgrade, Serbia

[b]Institute of Nuclear Sciences Vinca, Belgrade, Serbia

Pure and 10 mol% Fe^{3+} doped CeO_2 nanocrystals were synthesized by hydrothermal method using two different basic solutions (NH_4OH and NaOH). All the samples were calcinated at 140 ℃ and 200 ℃. The characterization of crystalline structure, vibrational and optical properties was performed using X-ray diffraction, Raman spectroscopy and spectroscopic ellipsometry. The obtained results showed that the Fe-doped samples are solid solutions with different size of nanocrystals, very dependent on the synthesis temperature and type of basic solution. The Raman measurements demonstrated electron molecular vibrational coupling and increase of oxygen vacancy concentration whereas doping provokes a small decrease of optical absorption edge in comparison with pure ceria.

PACS numbers: 81.16.Be, 61.05.C−, 78.30.−j, 78.67.Bf

1. Introduction

Ceria (CeO_2) as a material with relatively high dielectric constant attracted renewed interest as a capacitor dielectric in dynamic random access memories (DRAMs) and as resistive oxygen sensor [1]. It is a potential electrolyte for intermediate temperature solid oxide fuel cells (ITSOFCs) and recently it became a promising material for the second generation of spintronics due to the observed room- temperature ferromagnetism [2, 3].

CeO_2 nanocrystals and their solid solutions that are substituted with Fe^{3+} ions have been prepared by various methods such as sol–gel [4], hydrothermal synthesis [5], conventional mixed-oxide method [6] and ball--milling process [7]. It was found that ferromagnetic and photocatalytic properties as well as grain growth stabilization at higher temperatures can be significantly improved by doping CeO_2 nanocrystals with transition metal elements such as Fe [7–9]. But still one of the major challenges for the preparation techniques remains the precise control of particle size.

The aim of this work was to present relatively new and cost-effective hydrothermal method for obtaining ceria nanopowders and to investigate the influence of the synthesis parameters on the structural and optical properties of pure and 10 mol% Fe^{3+} doped CeO_2 nanopowders.

2. Experiment

Hydrothermal method has been employed to synthesize CeO_2 nanoparticles from $Ce(SO_4)_2{\cdot}4H_2O$ (Acros Organics) precursor with $FeCl_3{\cdot}6H_2O$ as dopant in NH_4OH (Carbo Erba) or NaOH (MP Hemija) solution. At the first stage of synthesis we converted $FeCl_3{\cdot}6H_2O$ to $Fe_2(SO_4)_3$ by H_2SO_4 (Zorka). The $Ce(OH)_4$ hydrogel was obtained by hydrolysis at room temperature with controlled addition of basic solution to the aqueous solution of 0.4 M $Ce(SO_4)_2$. During the process of hydrolysis, Ce^{4+} ions are hydrolyzed forming complexes with water molecules or OH^- to give the $[Ce(OH)_x(H_2O)_y]^{(4-x)+}$ complex, where $x+y$ is the coordination number of Ce^{4+}. In an aqueous solution, polar molecules of H_2O tend to take protons away from coordinated hydroxide, leading to the formation of $CeO_2 \cdot nH_2O$ [10]. This process can be described by the following equations [11]:

$$Ce^{4+} + xOH + yH_2O \rightarrow [Ce(OH)_x(H_2O)_y]^{(4-x)+1}, \quad (1)$$

$$[Ce(OH)_x(H_2O)_y]^{(4-x)+} + H_2O \rightarrow CeO_2 \cdot nH_2O + nH_2O + H_3O^+. \quad (2)$$

The final volume ratio of NH_4OH or NaOH solution and $Ce(SO_4)_2$ is about 1:5 and pH value (9.4) was kept fixed. Cerium sulfate is soluble in water but all experiments were carried out using a magnetic stirrer which gave more uniform concentration. As-prepared pure $Ce(OH)_4$ or 10 mol% Fe doped hydrogels were filtered and washed out with distilled water. Absence of SO_4^{2-} ions was controlled by standard procedure (0.1N solution of $BaCl_2$, Merck). Hydrogels were dried in the oven at 80 ℃ yielding the powdered material. The obtained powders were calcinated at 140 ℃ and 200 ℃ and after that were converted to nanocrystals.

The X-ray diffraction (XRD) patterns were collected at room temperature using Siemens D5000 diffractometer with Cu K_α radiation. Diffractograms of the nanocrys-

* corresponding author; e-mail: marrad@ipb.ac.rs

talline CeO_2 samples were recorded over the 2θ range from 20° to 80°. Raman scattering measurements were performed at room temperature using the Jobin-Yvon T64000 triple spectrometer system equipped with a liquid-nitrogen cooled CCD detector. The $\lambda = 514.5$ nm line of an Ar^+ laser was used as an excitation source. Ellipsometric measurements were performed at room temperature in UV–VIS (2–5.5 eV) spectral range, using high resolution variable angle spectroscopic ellipsometer (SOPRA GES5E — IRSE) of the rotating polarizer type.

3. Results and discussion

In the process of preparing $Ce(OH)_4$ from precursor, two different bases were used (NaOH and NH_4OH) in order to try to investigate the influence of the basic solution on the $[Ce(OH)_x(H_2O)_y]^{(4-x)+}$ complex. Calcination, as one of the main parameters of hydrothermal process, has been carried out for temperatures of $T = 140$ ℃ and $T = 200$ ℃ with an aim to investigate the process of crystallization and grain growth from the very beginning, when CeO_2 nanopowders have distinct properties comparing to the bulk materials.

In Fig. 1 there are displayed XRD patterns for pure and 10 mol% Fe^{3+} doped CeO_2 samples. From the analysis of diffraction data we have concluded that all synthesized samples have fluorite type structure of CeO_2 and characteristic Miller indices are denoted for each diffraction peak in Fig. 1. Doping with 10 mol% Fe^{3+} induces small contraction of lattice parameter due to mismatch between ionic radii of Ce^{4+} and Fe^{3+} ions. Average particle size (Fig. 2) is calculated according to Scherrer equation [12] from XRD data presented in Fig. 1. With an increase of the calcination temperature from 140 ℃ to 200 ℃, particle size increases primarily due to the coalescence process [13]. Particle size for doped samples calcined at 200 ℃ increases significantly comparing to pure CeO_2 sample and specially in the case of Fe-doped sample prepared using NaOH solution.

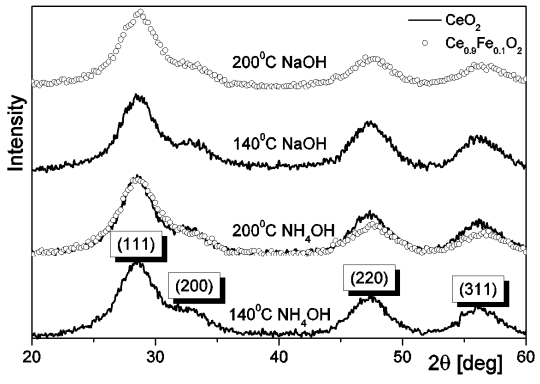

Fig. 1. X-ray diffraction patterns of pure and 10 mol% Fe^{3+} doped CeO_2 samples prepared at two different calcination temperatures (140 ℃ and 200 ℃) using two different basic solutions (NH_4OH and NaOH).

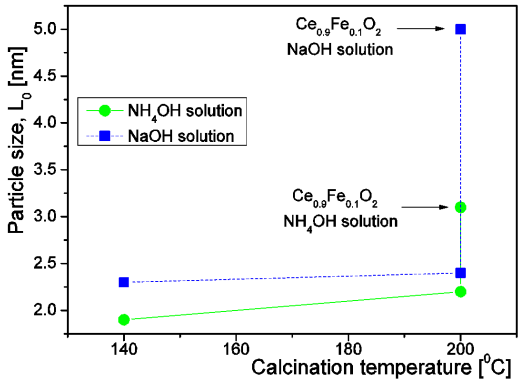

Fig. 2. Change of average particle size with calcination temperature for pure and 10 mol% Fe^{3+} doped CeO_2 samples.

In Fig. 3 there are presented room temperature Raman spectra of pure and 10 mol% Fe^{3+} doped CeO_2 samples. Main feature in the first order Raman spectrum of CeO_2 is triple degenerate F_{2g} mode. This mode in our nanocrystalline CeO_2 sample is located at ≈ 450 cm^{-1}. With increase in calcination temperature frequency of this mode increases and its line width decreases as a consequence of particle size growth [14]. Additional mode in the Raman spectrum is located at 600 cm^{-1}. This mode is ascribed to oxygen vacancies generated in CeO_2 lattice as a consequence of nonstoichiometry due to the small crystallite size. Doping with 10 mol% Fe^{3+} induces redshift and broadening of main F_{2g} mode. Such a behavior can be assigned to electron molecular vibrational coupling due to increased concentration of defects and magnetic ions in CeO_2 lattice. The intensity of the oxygen vacancy mode for pure and doped samples is determined by Lorentzian line shape fitting procedure. The change of the oxygen vacancy mode intensity with calcination temperature for pure and 10 mol% Fe^{3+} doped CeO_2 samples is presented in Fig. 4. As can be seen from Fig. 4, intensity of this mode is significantly higher for doped samples leading us to conclude that doping with Fe^{3+} ions induces higher disorder in oxygen sub-lattice and consequently higher concentration of oxygen vacancies. This is even more pronounced for Fe doped sample prepared with NH_4OH solution and calcinated at 200 ℃. Such a behavior is consistent with our expectations to have more unsaturated surface bonds and consequently higher concentration of defect states in comparison with the Fe-doped sample prepared from NaOH solution because of the great difference in crystallite size between these samples (see Fig. 2). The possibility of changing the oxygen vacancy concentration in ceria lattice varying the synthesis conditions can be very important fact because of the application of this material in oxygen transport technologies.

The results of spectroscopic ellipsometry for pure and 10 mol% Fe^{3+} doped CeO_2 samples are presented in Fig. 5a and b in the form of spectral dependence of in-

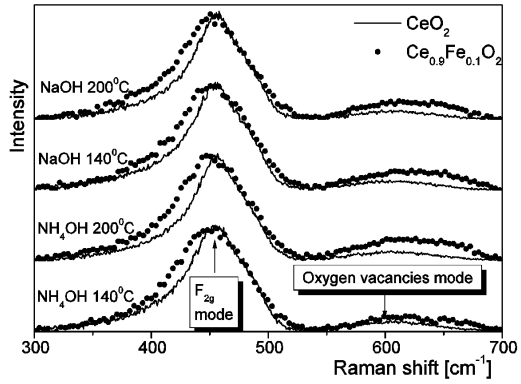

Fig. 3. Raman spectra of pure and 10 mol% Fe^{3+} doped CeO_2 samples.

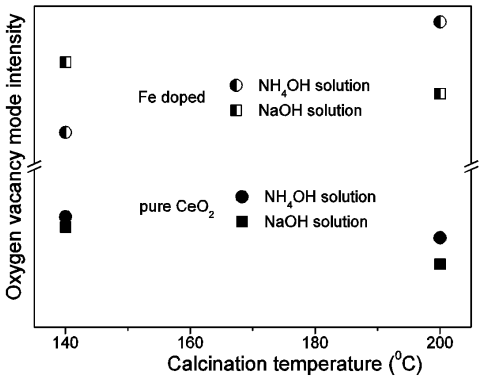

Fig. 4. Change of the oxygen vacancy mode intensity with calcination temperature for pure and 10 mol% Fe^{3+} doped CeO_2 samples.

dex of refraction and extinction coefficient in UV–VIS range. The refractive index (n) and extinction coefficient (k) of pure and doped samples were obtained by direct inversion of measured spectroscopic angles Ψ and Δ using very simple two-phase model (nanocrystalline CeO_2/air) [15]. Difference in spectral dependence of n and k indicates that optical parameters of CeO_2 nanoparticles are strongly correlated to the synthesis parameters [16, 17] (which in our case are type of basic solution and calcination temperature).

The direct optical band gap (E_g) was evaluated from the general equation [15]:

$$\alpha E = b(E - E_g)^{1/2}, \tag{3}$$

where α is the absorption coefficient related to the extinction coefficient k and photon wavelength λ ($\alpha = 4\pi k/\lambda$), E is photon energy and parameter b is related to the density of states in the conduction band. The plot of $(\alpha\ E)^2$ versus E for pure and 10 mol% Fe^{3+} doped CeO_2 samples is shown in Fig. 6. The values of the optical band gap lie in the range of 3.33–3.38 eV for the pure CeO_2 and in the range 3.26–3.33 eV for Fe doped samples. By analyzing the absorption behavior we can observe that

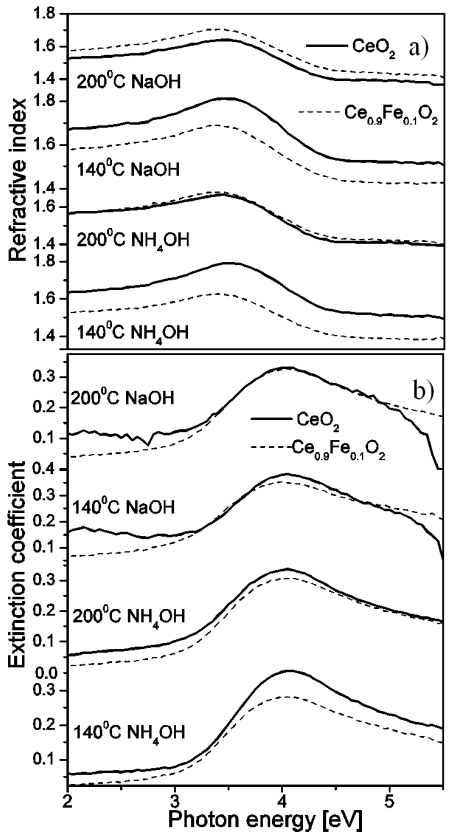

Fig. 5. Spectral dependence of the (a) refractive index and (b) extinction coefficient for pure and 10 mol% Fe^{3+} doped CeO_2 samples.

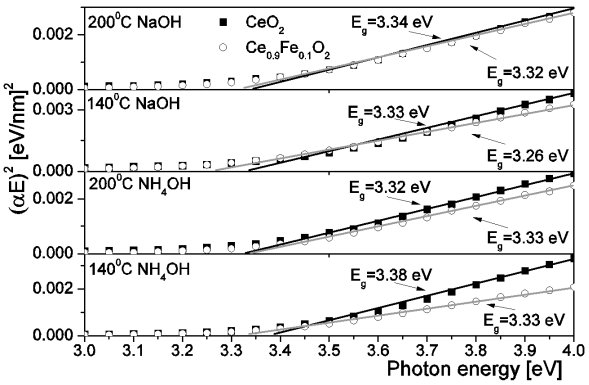

Fig. 6. The behavior of $(\alpha E)^2$ as a function of photon energy (symbols) together with linear fit (solid lines) according to Eq. (3) for pure and 10 mol% Fe^{3+} doped CeO_2 samples.

doping with 10 mol% Fe^{3+} provokes a small decrease of band gap value — E_g, in comparison with pure ceria, due to additional states introduced within the band gap. These states are originating from oxygen vacancy defect states [18] and electronic states of Fe^{3+} ions.

4. Conclusion

The hydrothermal method has been successfully employed to synthesize CeO_2 and $Ce_{0.9}Fe_{0.1}O_2$ nanocrystals using NH_4OH and NaOH solutions. XRD analysis showed that 10 mol% Fe doped samples are solid solutions with different average nanocrystal size dependent on the synthesis temperature and type of basic solution. From the Raman spectroscopy we observed strong influence of particle size effects on vibrational properties of pure CeO_2 nanocrystals while for 10 mol% Fe^{3+} doped samples we observed electron molecular vibrational coupling and increase of oxygen vacancy concentration. Ellipsometric measurements showed that optical properties of CeO_2 nanoparticles are strongly correlated to synthesis parameters whereas doping with Fe^{3+} ions provokes a small decrease of optical absorption edge in comparison with pure ceria. Monitoring and controlling the shift of optical band gap in ceria based nanomaterials can have significant implications in electronic and optoelectronic technologies.

Acknowledgments

This work was supported by the Ministry of Science and Technological development of Republic of Serbia under the project No. 141047 and SASA project F-134.

References

[1] N. Izu, W. Shin, I. Matsubara, N. Murayama, *Sens. Actuators B* **94**, 222 (2003).

[2] T. Matsui, M. Inaba, A. Mineshige, Z. Ogumi, *Solid State Ion.* **176**, 647 (2005).

[3] Q.Y. Wen, H.W. Zhang, Y.Q. Song, Q.H. Yang, H. Zhu, J.Q. Xiao, *J. Phys., Condens. Matter* **19**, 246205 (2007).

[4] F. Tessier, F. Chevré, F. Munoz, O. Merrdignac--Conanec, R. Marchand, M. Bouchard, C. Colbeau--Justin, *J. Solid State Chem.* **181**, 1204 (2008).

[5] K. Higashi, K. Sonoda, H. Ono, S. Sameshima, Y. Hirata, *Key Eng. Mater.* **159-160**, 25 (1999).

[6] T. Zhang, P. Hing, H. Huang, J. Kilner, *J. Eur. Ceram. Soc.* **21**, 2221 (2001).

[7] T.S. Zhang, J. Ma, L.B. Kong, Z.Q. Zeng, P. Hing, J.A. Kilner, *Mater. Sci. Eng. B* **103**, 177 (2003).

[8] L. Yue, X.-M. Zhang, *J. Alloy Comp.* **475**, 702 (2009).

[9] H. Bao, X. Chen, J. Fang, Z. Jiang, W. Huang, *Catal. Lett.* **125**, 160 (2008).

[10] M.L. Dos Santos, R.C. Lima, C.S. Riccardi, R.L. Tranquilin, P.R. Bueno, J.A. Varela, E. Longo, *Mater. Lett.* **62**, 4509 (2008).

[11] M. Hirano, M. Inagaki, *J. Mater. Chem.* **10**, 473 (2000).

[12] M. Birkholz, *Thin Film Analysis by X-Ray Scattering*, Wiley-VCH, Weinheim 2006, p. 85.

[13] W.J. Zhang, D.E. Miser, *J. Nanopart. Res.* **8**, 1027 (2006).

[14] Z.D. Dohčević-Mitrović, M. Radović, M. Šćepanović, M. Grujić-Brojčin, Z.V. Popović, B. Matović, S. Bošković, *Appl. Phys. Lett.* **91**, 203118 (2007).

[15] H.G. Tompkins, E.A. Irene, *Handbook of Ellipsometry*, William Andrew Publ., Norwich 2005.

[16] S. Guo, H. Arwin, S.N. Jacobsen, K. Järrendahl, U. Helmersson, *J. Appl. Phys.* **77**, 5369 (1995).

[17] E.E. Khawaja, S.M.A. Durrani, M.F. Al-Kuhaili, *J. Phys. D, Appl. Phys.* **36**, 545 (2003).

[18] F. Marabelli, P. Wachter, *Phys. Rev. B* **36**, 1238 (1987).